Journal of Colloid and Interface Science **247,** 372–380 (2002)
doi:10.1006/jcis.2001.8156, available online at http://www.idealibrary.com on IDEAL®

Sliding of Liquid Drops Down an Inclined Solid Surface

Ho-Young Kim,*,[1] Heon Ju Lee,* and Byung Ha Kang†

*Thermal/Flow Control Research Center, Korea Institute of Science and Technology, Seoul 136-791, Korea; and †School of Mechanical and Automotive Engineering, Kookmin University, Seoul 136-702, Korea

E-mail: hoyoung@kist.re.kr

Received April 30, 2001; accepted December 10, 2001

A liquid drop that partially wets a solid surface will slide down the plane when it is tilted beyond a critical inclination. Here we report the study of the sliding velocity of such a drop. Experiments for measuring the steady sliding velocity of different liquids of drops are performed. We then construct a scaling law that predicts the sliding velocity given the physical properties, wetting characteristics, and size of the drop. When the sliding velocity is low and the drop distortion due to inclination is small, the scaling law is shown to correctly model the functional dependency of the measured sliding velocity.

Key Words: **liquid drop; sliding; scaling law; capillary; wetting.**

1. INTRODUCTION

When a liquid drop is placed on a tilted solid plane, the drop tends to move down the incline. A drop on a superhydrophobic surface will roll down the plane (1, 2) but a drop that partially wets the surface will seemingly slide along the surface. At a small inclination angle, however, the drops stick to a solid surface. From a continuum point of view, the mechanism responsible for this drop adhesion is described in terms of the contact angle hysteresis, i.e., the difference between the advancing contact angle and the receding contact angle. The onset of the contact line's motion, i.e., the transition from its pinned state to a moving state, is regarded as a dynamic critical phenomenon that occurs when the energy barrier due to a defect is overcome (3, 4).

Here we consider the motion, beyond the critical state, of a partially wetting viscous drop under the gravitational field Despite its frequent appearance in natural processes such as a raindrop hitting a windowpane and in engineering applications including condensing vapor on a cold tube surface, the problem of a sliding drop has attracted only a limited attention to date (5–8). In this problem, the classical no-slip boundary condition leads to a divergence in the shear stress and the energy dissipation at the contact line where the three phases of solid/liquid/gas meet (9). Another famous droplet motion involving the contact line movement is the spreading of drops on a horizontal surface. Although the spreading problem also suffers from the contact line singularity, relatively plentiful studies have been reported (10–18) for this problem, and this is partially attributed to the fact that the problem is essentially axisymmetric, thus two-dimensional. Moreover, Refs. (19–21) assume that the spreading drop approximates a cylindrical disk to obtain a closed-form expression for the spreading velocity and the dynamic contact angle, which was hardly possible by those general two-dimensional models. On the other hand, a sliding drop down an incline tends to distort from its sessile configuration and describing this three-dimensional drop shape, let alone its movement, requires a considerable effort (22). This aggravates the difficult of the sliding drop problem together with the contact line singularity.

At the moving contact line, one needs to set up such boundary conditions that determine the behavior of the contact angle and remove the shear-stress singularity (23). Here we briefl review the boundary conditions set up in the previous models for the "sliding" drop. Hocking (5) examined the sliding drop assuming a thin two-dimensional configuration At the contact line, the advancing and receding contact angles were fi ed at small values. To relieve the singularity, his analysis used a Navier slip model (24) that the slip velocity is linearly proportional to the local velocity gradient, or the shear stress, at the drop bottom in contact with a solid surface. Dussan V. and Chow (6) and Dussan V. (7) obtained asymptotic solutions for a steady movement of a drop in the limit of both the Reynolds number and the capillary number approaching zero. Hence, these studies obtained the contact line motion as a perturbation to a quasi-static solution. At the contact line, a linear variation of the dynamic contact angles with the speed of the contact line was assumed. The models do not suffer from the shear-stress singularity since they were limited to the case as the capillary number approaches zero. Durbin (8) also analyzed the sliding of a thin two-dimensional drop assuming fi ed advancing and receding contact angles. In the model, the velocity slip was assumed in a so-called yield stress region near the contact line, where the shear stress was held constant at the interface's yield stress. Let alone the validity of those models, these studies are concerned only with limited configurations e.g., small thin drops that enable

[1] To whom correspondence should be addressed.

0021-9797/02 $35.00

the lubrication approximation; hence general understanding on this problem, including partially wetting drops, is still far from complete.

In this work, we perform experiments to measure the steady velocity of partially wetting viscous drops down an inclined solid surface. The measurement data for the sliding velocity of partially wetting drops appear rare, although the rolling velocity of a drop on a superhydrophobic surface has been reported (2). Furthermore, an approximate model for predicting the functional dependency of the sliding velocity on various parameters is constructed. To this end, we employ the theory of de Gennes (3) and de Ruijter *et al*. (21) to evaluate the dissipation during the drop motion. In addition, we approximate the shape of a sliding drop, in a similar spirit to Refs. (19–21) for a spreading drop, to obtain the closed-form expression of the sliding velocity.

2. EXPERIMENTS

2.1. Dependency of the Sliding Velocity

We consider a drop whose center of mass moves with a steady velocity U down a plane inclined at an angle α with the horizontal as shown in Fig. 1. It is first necessary to determine which parameters affect the drop sliding velocity in order to achieve meaningful experimental measurements. To this end, we perform dimensional analysis (25) to obtain the functional dependency of similarity variables relevant to our system. The drop has the density ρ, the surface tension σ, and the viscosity μ, with its radius R_0 when in a spherical shape. We assume that U is dependent upon R_0, σ, μ, the gravitational force per volume, $\rho g \sin\alpha$ with g being the gravitational acceleration, and interfacial parameters. Here we let the interfacial parameters include the microscopic length scale, λ, which relieves the classical no-slip boundary condition at the contact line, and the static and dynamic contact angles. It is noted that different theories on the contact line dynamics may choose different sets of interfacial parameters. For example, the dynamic contact angles may be replaced by the proportional constants between the contact line speed and the difference of the dynamic and static contact angles (5, 6, 26). See Section 9 of (23) for more discussions on various theories of contact line dynamics. In addition, it is noted that we choose R_0 as a single length parameter under the assumption that the essential information on the drop geometry can be deduced based on R_0 and the interfacial parameters such as contact angles.

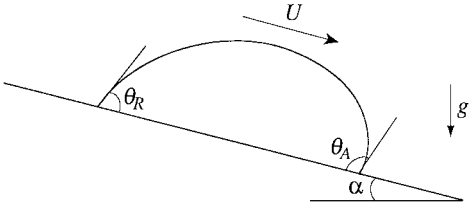

FIG. 1. Shape of a drop sliding down a surface inclined at α with the horizontal, having the advancing contact angle θ_A and the receding contact angle θ_R.

TABLE 1
Physical Properties of the Liquids Used in the Experiments

Liquid	Density (kg/m^3)	Viscosity (Pa · s)	Surface tension (N/m)	κ^{-1} (mm)	θ_e (°)
EG	1114	0.0209	0.0484	2.1	70.2
GW	1228	0.0600	0.0641	2.3	73.6
Glycerin	1260	0.95	0.063	2.3	78.1

Dimensional analysis reveals that the dimensionless velocity, i.e., the capillary number $\mathrm{Ca} = \mu U/\sigma$ is expressed as

$$\mathrm{Ca} = f(\mathrm{Bo_T}, \Pi_i), \qquad [1]$$

where $\mathrm{Bo_T}$ is the Bond number tangential to the inclined surface, $\mathrm{Bo_T} = \rho g R_0^2 \sin\alpha/\sigma$, and Π_i denotes the dimensionless interfacial parameters which include, under our current assumption, λ/R_0, the equilibrium contact angle θ_e, the advancing contact angle θ_A, and the receding contact angle θ_R. In our experiments, we use different drop liquids to vary the fluid-dynamic and interfacial properties. In addition, various volumes of drops are tested to investigate the effects of the drop size, and the inclination is changed to vary the gravitational force component.

2.2. Description of the Experimental Apparatus

The liquids used in the present study are ethylene glycol (EG: above 99.5%), glycerin (80 wt%)–water (20 wt%) mixture (GW), and glycerin (above 98.5%). The physical properties of the liquids are shown in Table 1 with their capillary lengths κ^{-1}. The drops are placed on solid surfaces using a pipette (Gilson Pipetman P1000). Polycarbonate is used as a solid surface, and its root-mean-square (RMS) surface roughness is measured to be 1.3 nm with 4.8% of standard deviation (27). To deduce the mass of a liquid drop, the weight of the solid substrate before and after placing a drop on it is measured using an electronic analytical balance (Mettler-Toledo AB204-S). The solid substrate is then placed on a plane, which can be tilted by rotating a handle as shown in Fig. 2. A ruler is attached to the apparatus to deduce the tilt angle of the plane.

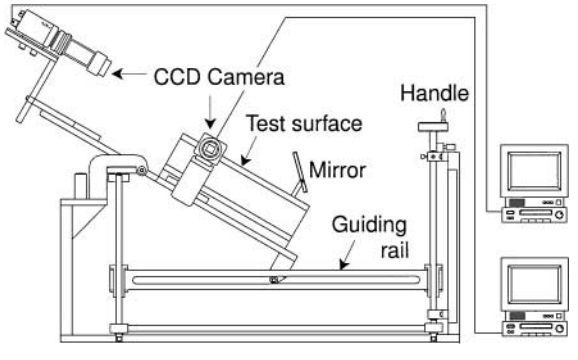

FIG. 2. A schematic of the experimental setup.

The equilibrium contact angles are measured using the same method as employed in (28), and the values are listed in Table 1. We then measure a critical angle of inclination at which a drop, strictly speaking, a trailing edge of the drop, starts to move. To observe the trailing edge from the side, a high-magnif cation zoom lens (Moritex ML-Z07545) is attached to a CCD camera (Pulnix TM-200). The ruler on the experimental apparatus is read at the moment the trailing edge starts to move while slowly rotating the handle. The critical inclinations for various volumes of drops of each liquid are measured.

In experiments to investigate the motion of a drop, the plane is tilted to an angle greater than the critical inclination, and then stopped. After the drop moves a distance greater than twice its base diameter, the plane is tilted further to observe the drop motion at an increased tilt angle. The same procedure is repeated until the drop moves out of the f eld-of-view of the CCD cameras. Two CCD cameras are used to obtain both the top and side views, and they are f xed to the tilting plane to get stationary f elds-of-view while the plane is inclined. S-VHS video cassette recorders (Philips VR999/61) are connected to the cameras to record the images. Each camera is equipped with a magnifying lens (Computer MLH-10X). During experiments, both images are displayed on monitors (Sony PVM-14N5E). After experiments, images are digitized by a frame grabber (Eurecard Picolo Pro2) and analyzed using an image analysis software. Figure 3 shows a typical image of a sliding drop observed in the experiments. The volumes of drops are varied in the range of about 15 to 85 mm^3; i.e., R_0 varies between 1.5 and 2.7 mm.

From the side-view images, we measure the length and the height of the drop and the speeds of both advancing and receding edges of the drop. The width of the drop is measured from the top-view images. A ruler recorded by the same video setup is used for calibration. Figure 4 shows the typical measurement data for the drop's traveling distance versus time, which indicates that the drop moves steadily during experiment.

2.3. *Experimental Results*

As discussed above, the sliding velocity depends on various parameters and even dimensional analysis reveals multiple dimensionless variables on which the dimensionless velocity depends. It is the objective of this work that we experimentally investigate the dependency of the velocity on those various parameters and that we construct a scaling law to explain the observed phenomena. In this section, we f rst present the selected measurement data obtained for various experimental conditions

FIG. 3. Image of an EG drop on a sold surface tilted close to its critical inclination. The drop volume is 13.4 mm^3 and the inclination is 12°.

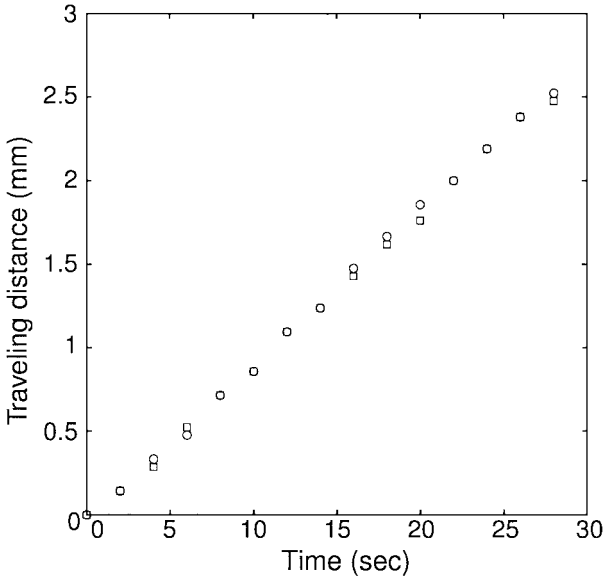

FIG. 4. Measurement results of a typical traveling distance of a glycerin drop versus time. Circles and squares denote the advancing and receding contact lines, respectively. For the case shown here, the drop volume is 77.8 mm^3 and the inclination angle is 20°.

in Table 2. A complete set of experimental data will be used in the plots drawn later when the scaling law is employed to organize them. A theoretical development to elucidate the mechanism that governs the steady sliding of viscous drops follows below.

TABLE 2
Selected Experiment Conditions and Measurement Results for the Steady Sliding Velocity

Liquid	Volume (mm^3)	α (°)	U (mm/s)
EG	15.1	14	0.229
		15	0.352
		20	0.649
		25	1.234
		30	1.724
		36.5	1.799
	29.2	9.5	0.158
		11	0.375
		14	0.643
		15	0.951
		18	1.187
		20	1.557
GW	24.0	20	0.122
		21.5	0.184
		22.5	0.275
		25	0.399
		28	0.490
		30	0.667
Glycerin	77.8	14	0.041
		15	0.065
		18	0.070
		20	0.092
		22.5	0.102
		28	0.132

3. ANALYSIS OF SLIDING VELOCITY

3.1. Energy Balance

We construct a scaling law for the steady velocity of a sliding drop based on the energy balance. The motion is driven by the gravitational field and we write the rate of decrease of the gravitational potential energy, Φ_g, as

$$\Phi_g = \rho V g U \sin\alpha, \qquad [2]$$

where V is the volume of the drop. To enable the steady motion of a drop, the gravitational energy decrease should be dissipated during its motion. Following de Gennes (3), the total dissipation function Φ_t can be written as

$$\Phi_t = \Phi_v + \Phi_l + \Phi_f, \qquad [3]$$

where Φ_v denotes the viscous dissipation due to the velocity field in the continuum domain and is detailed in next subsection. Φ_l is the dissipation in the vicinity of the contact line associated with the motion of fluid molecules between adsorption sites distributed on the solid surface (21, 29). The dissipation in the precursor film, Φ_f, is neglected since we are dealing with a partial wetting regime where the appearance of the precursor film is not probable (21).

In the vicinity of the contact line, its movement can be viewed as the motion of fluid molecules to the neighboring adsorption sites on a solid (21, 29). The dissipation associated with this microscopic process is denoted by Φ_l, and it is the sum of the dissipation at the advancing edge $\Phi_{l,A}$ and that at the receding edge $\Phi_{l,R}$, i.e., $\Phi_l = \Phi_{l,A} + \Phi_{l,R}$. First we consider the dissipation at the advancing contact line which is given by

$$\Phi_{l,A} = \int_{L_A} q U_n \, dl, \qquad [4]$$

where L_A is the length of the advancing contact line and U_n is the velocity component normal to the contact line written as $U_n = U\cos\beta$, where β is the azimuthal angle measured from the foremost advancing front of the drop. In addition, q is the work done by the force causing the contact line to move per unit displacement of unit length. References (29, 30) suggest that the jumping of fluid molecules between the adsorption sites is caused by the out-of-balance surface tension acting on the contact line; thus we write $q = \sigma(\cos\theta_e - \cos\theta_A)$. When the same mechanism is applied to the receding contact line and assuming that the advancing and receding edges are of the similar shape, Φ_l is given by

$$\Phi_l = \sigma U \int_0^{2\pi} x\cos\beta(\cos\theta_R - \cos\theta_A)\, d\beta. \qquad [5]$$

In general, x, θ_R, and θ_A are functions of the azimuthal angle β. Moreover, θ_R and θ_A are known to be dependent on the velocity U. However, it is reported that for low Ca, $\mathrm{Ca} \ll 10^{-2}$, the variation of the dynamic contact angle from its critical value at the onset of the motion is small (31, 32). As shown in the previous section, our experimental results fall in this low Ca regime, and the investigation of the drop images confirmed an insignificant change of the dynamic contact angles. Thus we assume that the dynamic contact angles at the critical inclination can be used to evaluate Φ_l with a sufficient accuracy for the present purpose of scaling analysis. Now it is noted that at the critical inclination α_c, the gravitational force parallel to the incline, $\rho V g \sin\alpha_c$, is balanced with the capillary force F_c (6, 33):

$$F_c = \int_0^{2\pi} x\cos\beta(\cos\theta_R - \cos\theta_A)\, d\beta. \qquad [6]$$

Therefore, Φ_l is written as, based on Eqs. [5] and [6],

$$\Phi_l = \rho V g U \sin\alpha_c. \qquad [7]$$

A further simplification, though approximate, of Eq. [6] is possible based on Ref. (22)'s computation result that the advancing (receding) contact angle of an inclined drop is constant for a wide range in the advancing (receding) edge, exhibiting an acute jump of the angle where the advancing and receding edges meet. In addition, when the drop/solid contact area is close to a circle, we get

$$F_c \approx \sigma w(\cos\theta_R - \cos\theta_A), \qquad [8]$$

where w is the width, or diameter, of the contact area. In this case,

$$\Phi_l \approx \sigma w U(\cos\theta_R - \cos\theta_A). \qquad [9]$$

It is interesting to note that the dissipation process near the contact line is directly related to the contact angle hysteresis. We find that this is consistent with the viewpoint of (34) that the contact angle hysteresis is associated with the liquid–solid adhesion.

3.2. Viscous Dissipation

The viscous dissipation is determined by the velocity field in the drop. When the drop is large, it consists of a flat central part mainly governed by gravity and an edge where the capillarity takes effect (35). In this case, the velocity field in the flat part may be assumed to obey the lubrication approximation, whereas the velocity field in the edge must be described using the Stokes equation unless the contact angle is very small (5). On the other hand, a small drop, whose characteristic size (e.g., the radius of its spherical form, R_0) is smaller than the capillary number, $\kappa^{-1} = (\sigma/\rho g)^{1/2}$, takes a spherical-cap shape on a horizontal solid surface. Provided that the drop deformation due to tilting of the solid surface is small and that the drop partially wets the solid surface, the entire flow field in the drop would follow

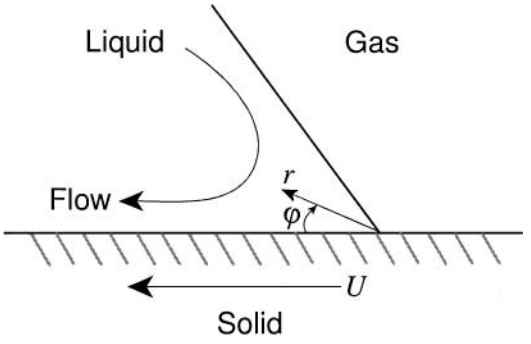

FIG. 5. The coordinate system and the flow field in a wedge near the contact line.

the Stokes equation. A criterion to determine a drop size below which the dissipation by the Stokes flow dominates is derived below.

We first compute the viscous dissipation by the Stokes flow in the wedge. This geometry models not only the edge of a large drop but also the entire volume of a small drop. Huh and Scriven (9) calculated the velocity field of a two-dimensional wedge satisfying the Stokes equation using the plane polar coordinates as shown in Fig. 5. The viscous dissipation per unit volume, f, in the plane polar coordinates is written as

$$f = 2\mu\left[\left(\frac{\partial v_r}{\partial r}\right)^2 + \left(\frac{1}{r}\frac{\partial v_\theta}{\partial \theta} + \frac{v_r}{r}\right)^2 + \frac{1}{2}\left(\frac{1}{r}\frac{\partial v_r}{\partial \theta} + \frac{\partial v_\theta}{\partial r} - \frac{v_\theta}{r}\right)^2\right], \quad [10]$$

where v_r and v_θ denote the radial and azimuthal velocities, respectively. Using the velocity field obtained by Huh and Scriven (9), it can be shown that f is given by

$$f = 4\mu\frac{U^2}{r^2}(a\cos\varphi - b\sin\varphi)^2, \quad [11]$$

where $a = \sin^2\theta/(\theta - \sin\theta\cos\theta)$ and $b = \sin\theta\cos\theta/(\theta - \sin\theta\cos\theta)$, θ being the contact angle. The dissipation in the liquid wedge per unit depth, Φ'_w, is then calculated as

$$\Phi'_w = \int_\lambda^\Lambda \int_0^\theta f r\, dr\, d\varphi, \quad [12]$$

where Λ is the length scale up to which the wedge flow approximation holds. A cutoff length λ is introduced to prevent a blowup of the dissipation (3, 35). In other words, the classical hydrodynamic theory ceases to hold in a region near the contact line whose size is represented by λ. A discussion on its magnitude is given later in this article, but it is known to range in a microscopic scale.

Substituting Eq. [11] into Eq. [12] yields

$$\Phi'_w = 4\mu U^2 c(\theta)\ln\left(\frac{\Lambda}{\lambda}\right), \quad [13]$$

where $c(\theta)$ is a function of the contact angle as plotted in Fig. 6. When θ is very small, the dissipation is quite severe. As θ approaches 180°, $c(\theta)$ vanishes, and so does the wedge dissipation. This case corresponds to a rolling of a small drop in which there is no singularity in either the force or the stress at the contact line (1). However, when θ falls in a moderate range, i.e., $0 \ll \theta \ll 180°$, $c(\theta)$ can be approximated to a linearly decreasing function within a sufficiently narrow angle range with its order remaining as unity. The partially wetting drop, which is of our interest here, belongs to this moderate contact angle range. Therefore, integrating Φ'_w over the drop perimeter, the wedge dissipation, Φ_w, is scaled as

$$\Phi_w \sim c(\theta)\mu U^2 L\ln\left(\frac{\Lambda}{\lambda}\right), \quad [14]$$

where $\sim$ means "on the order of" and L is the peripheral length of the drop/solid contact area. Here we have assumed that the viscous dissipation in the wedge can be estimated via a two-dimensional approximation. In addition, θ_e can be used for a representative contact angle θ either when dynamic contact angles do not deviate severely from the equilibrium contact angle or when the arithmetic mean of the advancing and receding contact angles is close to θ_e (5), recalling the locally near-linear behavior of $c(\theta)$.

The viscous dissipation obtained above accounts for the dissipation arising in the entire volume of a small drop. However, a

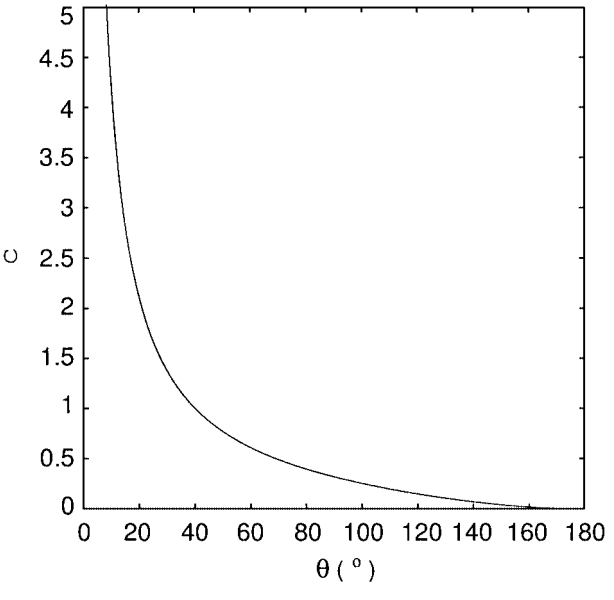

FIG. 6. c versus θ.

large drop experiences the dissipation by a lubrication f ow in its central part as well as the dissipation in its edge. The dissipation due to a bulk motion in the central part is denoted by Φ_b, and is scaled as

$$\Phi_b \sim \mu \int_{V_b} (\nabla \bar{v})^2 \, dV, \qquad [15]$$

where V_b is the volume of the central part and $\bar{v}$ the velocity f eld in the drop. The velocity gradient of the bulk motion in the drop is scaled as $|\nabla \bar{v}| \sim U/h$, where h is the height of the drop. Therefore, the order of magnitude of Φ_b is estimated as

$$\Phi_b \sim \mu V_b (U/h)^2. \qquad [16]$$

For a drop much larger than the capillary length, the height of the drop is given by (35)

$$h_0 = [2(7 - \cos\theta)]^{1/2} \kappa^{-1}. \qquad [17]$$

Now we compare the magnitudes of the wedge dissipation and the bulk dissipation for a large drop. If the contact area of a drop with a solid surface, or drop base area, is denoted by A_b, both V and V_b can be scaled as $A_b h$. In addition, if the drop base area is kept nearly circular despite the tilting of the plane, we write $L \sim 2\pi R_b$ and $A_b \sim \pi R_b^2$, R_b being the radius of the drop base area. Therefore, using Eqs. [14] and [16], the ratio Φ_b/Φ_w for a large drop is given by

$$\frac{\Phi_b}{\Phi_w} \sim \frac{R_b}{2hc(\theta)\ln(\Lambda/\lambda)}. \qquad [18]$$

If we scale the drop volume V as $V \sim \pi R_b^2 h$, Eq. [18] can be rewritten as

$$\frac{\Phi_b}{\Phi_w} \sim \left(\frac{R_0}{h}\right)^{3/2} \frac{1}{c(\theta)\ln(R_b/\lambda)}, \qquad [19]$$

where we let $\Lambda \sim R_b$. Therefore, it can be easily shown that when $R_0 \gg R_c$, Φ_b dominates over Φ_w and vice versa when $\kappa^{-1} \ll R_0 \ll R_c$, where the critical radius $R_c = h[\ln(R_b/\lambda)]^{2/3}$. As R_0 reduces to the similar order as κ^{-1}, the lubrication-f ow region vanishes and naturally the wedge f ow dominates.

Summarizing the foregoing evaluations of the viscous dissipation, we obtained the magnitudes of the two dissipation mechanisms, i.e., the wedge dissipation and the bulk dissipation. The wedge dissipation by the Stokes f ow accounts for the dissipation in the edge of a large drop or the dissipation arising in the entire volume of a small drop. The bulk dissipation by the lubrication f ow is due to a f uid motion taking place in the central part of a large drop. Therefore, the total viscous dissipation, Φ_v, is given by $\Phi_v \sim \Phi_w$ for a small drop ($R_0 \ll R_c$), and $\Phi_v \sim \Phi_w + \Phi_b$ for larger drops.

3.3. Steady Sliding Velocity

The steady velocity of a sliding drop is determined by the balance between the rate of change of gravitational potential energy and the dissipation: $\Phi_g = \Phi_l + \Phi_v$. First we consider a small drop ($R_0 \ll R_c$) in which the wedge dissipation is a dominant viscous dissipation mechanism. Using Eqs. [2], [7], and [14], the steady velocity U can be given by

$$U \sim \frac{\rho V g(\sin\alpha - \sin\alpha_c)}{\mu L c(\theta)\ln(\Lambda/\lambda)} \qquad [20]$$

or considering Eq. [9],

$$U \sim \frac{\rho V g \sin\alpha - \sigma w(\cos\theta_R - \cos\theta_A)}{\mu L c(\theta)\ln(\Lambda/\lambda)}. \qquad [21]$$

On the other hand, for larger drops, using $\Phi_v = \Phi_w + \Phi_b$, we get

$$U \sim \frac{\rho V g(\sin\alpha - \sin\alpha_c)}{\mu[V_b/h^2 + Lc(\theta)\ln(\Lambda/\lambda)]}. \qquad [22]$$

When a drop is extremely large, $R_0 \gg R_c$, the bulk dissipation dominates as discussed above and U is given by

$$U \sim \frac{h}{\mu A_b}[\rho V g(\sin\alpha - \sin\alpha_c)]. \qquad [23]$$

4. RESULTS AND DISCUSSION

4.1. Comparison with Previous Theoretical Results

Now we compare our scaling results with previous theoretical predictions (5–8). The most remarkable difference between the models of (5, 6, 8) and the current one is that our model is not restricted to a small contact angle assumption which enabled the lubrication approximation. The model of (7) does not assume a small contact angle, but it treats the problem as a perturbation to a static conf guration, neglecting the dynamic terms of the Navier–Stokes equation. It is noted that the moving contact line theory advanced by Shikhmurzaev (23) considers the general f ow conf guration not requiring the lubrication assumption. However, his analysis does not address the specif c problem of a drop sliding down an inclined plane, which is the subject of the present work.

Hocking's (5) linear solution for a small, thin two-dimensional drop is expressed as, in a dimensional form,

$$U = \frac{\theta_0^2}{9\mu \ln(2R_b\theta_0/3\tilde{\lambda})}\left(\rho g R_b^2 \sin\alpha - 3\sigma\theta_0\varepsilon\right), \qquad [24]$$

where $\tilde{\lambda}$ is the slip coeff cient corresponding to $\lambda\theta_0$ in the present case, where $\theta_0 = (\theta_A + \theta_R)/2$ (see Eq. (2.4) of Ref. (5)), and $\varepsilon = (\theta_A - \theta_R)/(\theta_A + \theta_R)$. To compare Eq. [24] with Eq. [21] in the case of a thin small drop, we rearrange Eq. [21] into a form

similar to that of Eq. [24]:

$$U \sim \frac{\theta_0}{\mu c(\theta_0)\ln(\Lambda/\lambda)}\left[\rho g R_b^2 \sin\alpha - \frac{8}{\pi}\sigma\frac{(\cos\theta_R - \cos\theta_A)}{\theta_0}\right]. \quad [25]$$

For $\theta \ll 1$, it follows that $c(\theta_0) \sim 1/\theta_0$. Letting $\theta_A = \theta_0 + \Delta\theta$ and $\theta_R = \theta_0 - \Delta\theta$, we get $\theta_0\varepsilon = \Delta\theta$ and $(\cos\theta_R - \cos\theta_A)/\theta_0 \sim 2\Delta\theta$ for $\theta_A, \theta_R \ll 1$. Therefore, Eq. [25] reduces to an almost identical form to Eq. [24] except for the coeff cient of a capillary term (the second term in the brackets).

Durbin's solution (8) can be expressed as in a dimensional form

$$U = \frac{\theta_0^2}{\mu \ln\left[2R_b\tau_c\theta_0(1-\varepsilon^2)^{1/2}/3\mu U\right]}\left(\rho g R_b^2 \sin\alpha - 3\sigma\theta_0\varepsilon\right), \quad [26]$$

where τ_c is the critical shear stress, over which the increase of shear stress is prevented by slip. Scaling $\tau_c \sim \mu U/\tilde{\lambda}$, where $\tilde{\lambda}$ is a length scale at which the shear stress reaches τ_c in this case, then Eq. [26] becomes identical to Eq. [24] for $\varepsilon \ll 1$.

Directly comparing the results of (6) and (7) with the current modeling is not possible since those results do not explicitly contain viscous effects. However, when the relationship between the contact line speed and contact angles are expressed as, following (6) and (7), $U = \kappa_A(\theta_A - \theta_{app})$ for an advancing line, where θ_{app} is the apparent contact angle, and as $U = \kappa_R(\theta_{app} - \theta_R)$ for a receding line, Hocking showed that for a thin small drop (5),

$$\kappa_A = \kappa_R = \frac{\sigma\theta_0^2}{3\mu\ln(2R_b/3\lambda)}. \quad [27]$$

Upon substituting Eq. [27] into Eq. (5.2) of Dussan V. (7), the equation becomes identical to Eq. [25] for $\theta_0 \ll 1$. Although the coeff cient of the capillary term in Hocking's result is different from that in our scaling result of Eq. [25], the capillary term of Dussan V.'s three-dimensional result has the same coeff cient as our scaling result when Eq. [27] is substituted. This is because the capillary term includes the width of the drop base area, w (see Eq. [9] or [21]), which could not be adequately accounted for in a two-dimensional theory of Hocking (5) while it was considered by Dussan V.'s theory (7). Therefore, we may expect that the primarily affected factor by extending Hocking's two-dimensional analysis to a three-dimensional conf guration would be the coeff cient of the capillary term that corresponds to the width of a drop base.

4.2. Comparison with the Experimental Results

Here we compare the experimental results listed in Table 2 with the scaling law constructed above. First we note that the critical radius R_c for each liquid, at which size the bulk dissipation and the wedge dissipation are of the same order, is so large that drops of this scale can hardly be observed in reality. For example, if we use κ^{-1} as a very conservative measure of h and of R_b, then R_c is calculated to be over 10 mm. In fact, drops of 20 mm diameter are not frequently encountered. Since the largest drop used in our experiments has a radius of 2.65 mm in its spherical form, the wedge dissipation is a dominant viscous dissipation mechanism. Thus, Eq. [20] is to be compared with the measurement results.

Equation [20] can be further simplif ed unless the drop "base" on a tilted plane deforms severely. In this case, we can approximate $L \approx 2\pi R_b$ and $\Lambda \approx R_b$, where R_b is the radius of the bottom contact area. Moreover, R_b can be approximated using its value taken by the drop on a horizontal surface, $R_{b,sc}$ as a function of R_0 and the equilibrium contact angle θ_c,

$$\frac{R_{b,sc}}{R_0} = \frac{4^{1/3}\sin\theta_e}{(2 - 3\cos\theta_e + \cos^3\theta_e)^{1/3}}, \quad [28]$$

where the subscript "sc" denotes "spherical cap." The validity of this spherical-cap approximation deteriorates as the size of the drop increases and the gravitational pull becomes more important, but our measurement results indicate that the largest underestimation error (at the maximum volume) caused by this assumption is about 15%. Therefore Eq. (20) can be written as

$$U \sim \frac{\rho g}{\mu c s}\Psi, \quad [29]$$

where $s(\theta_e) = R_{b,sc}/R_0$ and $\Psi = V^{2/3}(\sin\alpha - \sin\alpha_c)/\ln(R_b/\lambda)$. The most essential feature of the scaling analysis here is that the variation of the sliding velocity in response to changing parameters such as drop size and the inclination can be reduced to the relation as shown in Eq. (29). That is, U is a linear function of Ψ for a given liquid.

Figure 7 plots the steady sliding velocity of varying liquids versus Ψ. In evaluating Ψ, we set $\lambda = 10$ nm following the value taken by (13). This appears reasonable for our system considering that the size of the liquid molecules is below 1 nm and the RMS surface roughness is 1.3 nm. A further discussion on the scale of λ is given below. The f gure shows that all the liquids indeed exhibit a linear dependence of the sliding speed upon the parameter Ψ as predicted by our theory. The straight line drawn in each plot is from the least square method based on the experimental data. The fact that the line thus created nearly intersects with the origin implies that our evaluation of the critical inclination is highly accurate and compatible with our theory. We note that the slopes for each liquid are vastly different due to their different physical properties. Thus, we let $U = \gamma\rho g\Psi/\mu c s$ and compare the values of γ for each liquid after evaluating c and s for each liquid, which are assumed to be functions of the equilibrium contact angle only. The results are shown in Table 3, and we indeed f nd that the values of γ are close. This provides another experimental justif cation to our theory.

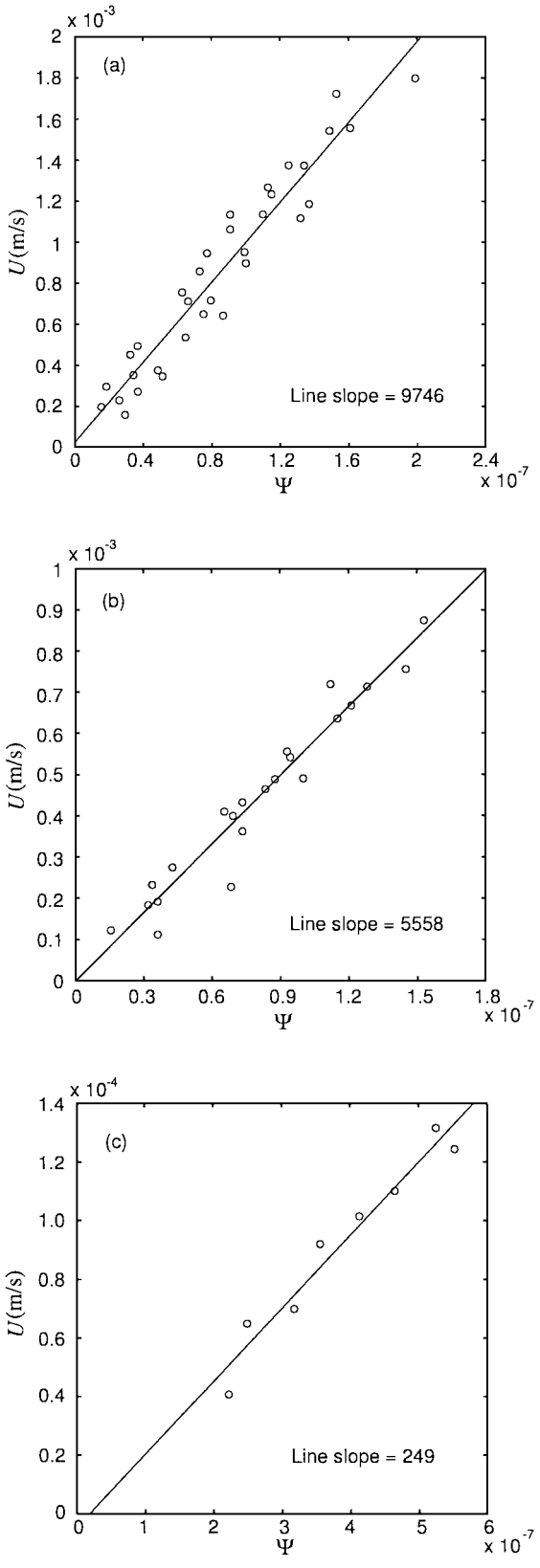

FIG. 7. The steady sliding velocity of liquid drops on an inclined surface plotted versus Ψ: (a) EG drops, (b) GW drops, and (c) glycerin drops.

TABLE 3
The Values of $c(\theta_e)$, $s(\theta_e)$, and γ

Liquid	c	s	γ
EG	0.488	1.48	1.3×10^{-2}
GW	0.454	1.44	1.8×10^{-2}
Glycerin	0.412	1.39	1.1×10^{-2}

As mentioned earlier, λ refers to a distance from a contact line below which the continuum mechanics theory ceases to hold. A conclusive agreement on the magnitude of λ does not seem to have been reached yet. However, the relevant studies report that the slip length, or a length scale at which the no-slip boundary condition breaks down, ranges between a few to a few hundred molecular diameters. This measures $O(1\text{ nm}) < \lambda < O(100\text{ nm})$ (13, 16, 18, 36), and its actual magnitude is also inf uenced by the interfacial parameters, such as the strength of the liquid–solid coupling and the thermal roughness of the interface. To quantify the sensitivity of the sliding velocity model to the magnitude of λ, we evaluate $\ln(R_b/\lambda)$ letting $R_b = 10^{-3}$ m. While λ varies between 1 and 100 nm, $\ln(R_b/\lambda)$ only changes by 33%, which is a very weak dependency considering two orders of variation in λ. In addition, it can be postulated that λ may vary according to the contact line velocity as other interfacial parameters such as dynamic contact angles. However, it seems reasonable to assume its variation to be small, considering a narrow range of Ca for each drop liquid. Therefore, it can be stated that the scaling law remains valid even though an accurate evaluation of λ is beyond the scope of the present work. Here we add that a similar insensitiveness of the drop "spreading" rate to the magnitude of λ was revealed by (13).

Recalling the dimensional analysis presented above, the dimensionless velocity Ca has such a functional dependency as shown by Eq. [1]. The relation reveals that the nondimensional independent parameters associated with the size (R_0) of a drop are only Bo_T and λ/R_0. Assuming that the variation of λ/R_0 is very small as discussed above, we may approximately determine Ca as a function of Bo_T for each liquid. Based on our experimental results, we plot Ca vs Bo_T as shown in Fig. 8. It suggests that Ca depends linearly on Bo_T, and this is explained by nondimensionalizing Eq. [20],

$$\text{Ca} \sim \frac{4\pi(\text{Bo}_T - \text{Bo}_{T,c})}{3\tilde{L}c\ln(\tilde{\Lambda}R_0/\lambda)}, \qquad [30]$$

where $\text{Bo}_{T,c} = \rho g R_0^2 \sin\alpha_c/\sigma$, $\tilde{L} = L/R_0$, and $\tilde{\Lambda} = \Lambda/R_0$. We can show that $\text{Bo}_{T,c}$ depends only on the interfacial parameter using Eq. [8] with $w = 2R_b$:

$$\text{Bo}_{T,c} = \frac{3}{2\pi}s(\theta_e)(\cos\theta_R - \cos\theta_A). \qquad [31]$$

References (33) and (37) experimentally showed that the contact angle hysteresis is independent of a drop size at the critical

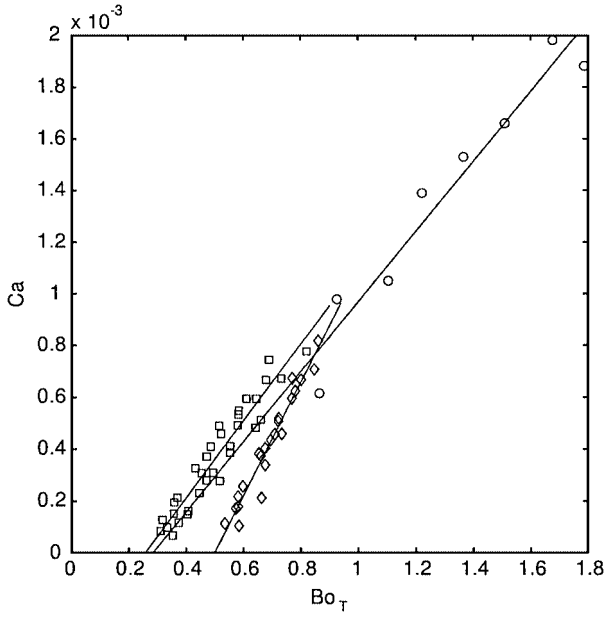

FIG. 8. Ca versus Bo_T for the measurement data obtained in this work. Squares denote EG drops, diamonds GW drops, and circles glycerin drops.

inclination. Then we find from Eq. [30] that as long as $\ln(\Lambda/\lambda)$ is kept nearly constant, Ca linearly depends on Bo_T with its slope determined by the interfacial parameters. Although this is obtained through the approximate modeling, it is first suggested to the authors' knowledge that the steady sliding velocity of a "partially wetting" viscous drop on a specific solid surface can be determined using a linear relation between Ca and Bo_T in a low-velocity regime.

5. CONCLUDING REMARKS

The sliding of liquid drops down an inclined solid surface is a complicated phenomenon that involves a three-dimensional distortion of a free surface and movement of both advancing and receding contact lines. Experimental measurement for the sliding velocity is essential to the advancement of our knowledge on this problem. In this work, we presented the experimental data for the sliding velocity of partially wetting viscous drops on a smooth solid surface. Furthermore, we constructed a scaling law that elucidates the functional dependence of the sliding velocity on various parameters. A simplifying assumption was made for the shape including the dynamic contact angles and the peripheral length for a region where Ca is kept low and the drop distortion due to tilting is small. In this regime, our scaling law correctly predicts the dependency of the measured sliding velocity on such parameters as the inclination and the drop volume, for each drop liquid. Especially, when the drop moves such that the logarithm for the ratio of the drop size to the microscopic cutoff length negligibly varies, we showed that Ca and Bo_T have a linear relation.

REFERENCES

1. Mahadevan, L., and Pomeau, Y., *Phys. Fluids* **11,** 1995 (1999).
2. Richard, D., and Quéré, D., *Europhys. Lett.* **48,** 286 (1999).
3. de Gennes, P. G., *Rev. Mod. Phys*. **57,** 827 (1985).
4. Schäffer, E., and Wong, P.-Z., *Phys. Rev. E* **61,** 5257 (2000).
5. Hocking, L. M., *Q. J. Mech. Appl. Math*. **34,** 37 (1981).
6. Dussan V. E. B., and Chow, R. T.-P., *J. Fluid Mech*. **137,** 1 (1983).
7. Dussan V. E. B., *J. Fluid Mech*. **151,** 1 (1985).
8. Durbin, P. A., *J. Fluid Mech*. **197,** 157 (1988).
9. Huh, C., and Scriven, L. E., *J. Colloid Interface Sci*. **35,** 85 (1971).
10. Hocking, L. M., and Rivers, A. D., *J. Fluid Mech*. **121,** 425 (1982).
11. Haley, P. J., and Miksis, M. J., *J. Fluid Mech*. **223,** 57 (1991).
12. Hocking, L. M., *J. Fluid Mech*. **239,** 671 (1992).
13. Gratton, R., Diez, J. A., Thomas, L. P., Marino, B., and Betelú, S., *Phys. Rev. E* **53,** 3563 (1996).
14. Shikhmurzaev, Y. D., *Phys. Fluids* **9,** 266 (1997).
15. Benintendi, S. W., and Smith, M. K., *Phys. Fluids* **11,** 982 (1999).
16. Barrat, J.-L., and Bocquet, L., *Phys. Rev. Lett*. **82,** 4671 (1999).
17. Voinov, O. V., *J. Colloid Interface Sci*. **226,** 22 (2000).
18. Pit, R., Hervet, H., and Léger, L., *Phys. Rev. Lett*. **85,** 980 (2000).
19. Seaver, A. E., and Berg, J. C., *J. Appl. Polym. Sci*. **52,** 431 (1994).
20. de Ruijter, M. J., De Coninck, J., Blake, T. D., Clarke, A., and Rankin, A., *Langmuir* **13,** 7293 (1997).
21. de Ruijter, M. J., De Coninck, J., and Oshanin, G., *Langmuir* **15,** 2209 (1999).
22. Dimitrakopoulos, P., and Higdon, J. J. L., *J. Fluid Mech*. **395,** 181 (1999).
23. Shikhmurzaev, Y. D., *J. Fluid Mech*. **334,** 211 (1997).
24. Lamb, H., "Hydrodynamics." Dover, New York, 1932.
25. Bridgman, P. W., "Dimensinal Analysis." Yale Univ. Press, New Haven, CT, 1931.
26. Greenspan, H. P., *J. Fluid Mech*. **84,** 125 (1978).
27. Kim, H.-Y., and Chun, J.-H., *Phys. Fluids* **13,** 643 (2001).
28. Schiaffino, S., "The Fundamentals of Molten Microdrop Deposition and Solidification." Ph.D. Thesis, MIT, Cambridge, MA, 1996.
29. Blake, T. D., and Haynes, J. M., *J. Colloid Interface Sci*. **30,** 421 (1969).
30. de Ruijter, M. J., Blake, T. D., and De Coninck, J., *Langmuir* **15,** 7836 (1999).
31. Hoffman, R. L., *J. Colloid Interface Sci*. **50,** 228 (1975).
32. Fermigier, M., and Jenffer, P., *J. Colloid Interface Sci*. **146,** 226 (1991).
33. Extrand, C. W., and Kumagai, Y., *J. Colloid Interface Sci*. **170,** 515 (1995).
34. Extrand, C. W., *J. Colloid Interface Sci*. **207,** 11 (1998).
35. Brochard-Wyart, F., Hervet, H., Redon, C., and Rondelez, F., *J. Colloid Interface Sci*. **142,** 518 (1991).
36. Thompson, P. A., and Robbins, M. O., *Phy. Rev. Lett*. **63,** 766 (1989).
37. Furmidge, C. G. L., *J. Colloid Sci*. **17,** 309 (1962).